Title

Intersectin1 promotes clathrin-mediated endocytosis by organizing and stabilizing endocytic protein interaction networks.

Journal

Cell Reports, 43(12)

Authors

Jin, Meiyan
Iwamoto, Yuichiro
Shirazinejad, Cyna
et al.

Publication Date

2024-12-24

DOI

10.1016/j.celrep.2024.114989

Peer reviewed

HHS Public Access

Author manuscript

Cell Rep. Author manuscript; available in PMC 2025 January 13.

Published in final edited form as:

Cell Rep. 2024 December 24; 43(12): 114989. doi:10.1016/j.celrep.2024.114989.

Intersectin1 promotes clathrin-mediated endocytosis by organizing and stabilizing endocytic protein interaction networks

Meiyan Jin[1,2,*], **Yuichiro Iwamoto**[1], **Cyna Shirazinejad**[1], **David G. Drubin**[1,3,*]

[1]Department of Molecular and Cell Biology, University of California, Berkeley, Berkeley, CA 94720, USA

[2]Department of Biology, University of Florida, Gainesville, FL 32611, USA

[3]Lead contact

SUMMARY

During clathrin-mediated endocytosis (CME), dozens of proteins are recruited to nascent CME sites on the plasma membrane, and their spatial and temporal coordination is crucial for efficient CME. Here, we show that the scaffold protein intersectin1 (ITSN1) promotes CME by organizing and stabilizing endocytic protein interaction networks. Live-cell imaging of genome-edited cells revealed that endogenously labeled ITSN1 is recruited during CME site stabilization and growth and that ITSN1 knockdown impairs endocytic protein recruitment during this stage. Targeting ITSN1 to the mitochondrial surface was sufficient to assemble puncta consisting of the EPS15 and FCHO2 initiation proteins, the AP2 and epsin1 (EPN1) adaptor proteins, and the dynamin2 (DNM2) vesicle scission GTPase. ITSN1 can form puncta and recruit DNM2 independent of EPS15/FCHO2 or EPN1. Our findings redefine ITSN1's primary endocytic role as organizing and stabilizing CME protein interaction networks rather than initiation, providing deeper insights into the multi-step and multi-zone organization of CME site assembly.

In brief

Jin et al. examined the spatiotemporal dynamics of endogenously labeled intersectin1 at clathrin-mediated endocytosis sites using a combination of imaging and computational approaches. They redefine intersectin1's function as stabilizing growing endocytic sites through its interaction with multiple key endocytic proteins, including dynamin2, AP2, EPS15, FCHO2, and epsin1.

*Correspondence: meiyan.jin@ufl.edu (M.J.), drubin@berkeley.edu (D.G.D.).

AUTHOR CONTRIBUTIONS

Conceptualization, M.J. and D.G.D.; methodology, M.J., Y.I., and C.S.; software, M.J., Y.I., and C.S.; validation, M.J., Y.I., C.S., and D.G.D.; investigation, M.J. and Y.I.; resources, M.J., C.S., and D.G.D.; data curation, M.J. and D.G.D.; writing – original draft, M.J.; writing – review & editing, M.J., Y.I., and D.G.D.; visualization, M.J., Y.I., and C.S.; supervision, D.G.D. and M.J.; funding acquisition, D.G.D. and M.J.

DECLARATION OF INTERESTS

The authors declare no competing interests.

SUPPLEMENTAL INFORMATION

Supplemental information can be found online at https://doi.org/10.1016/j.celrep.2024.114989.

Graphical Abstract

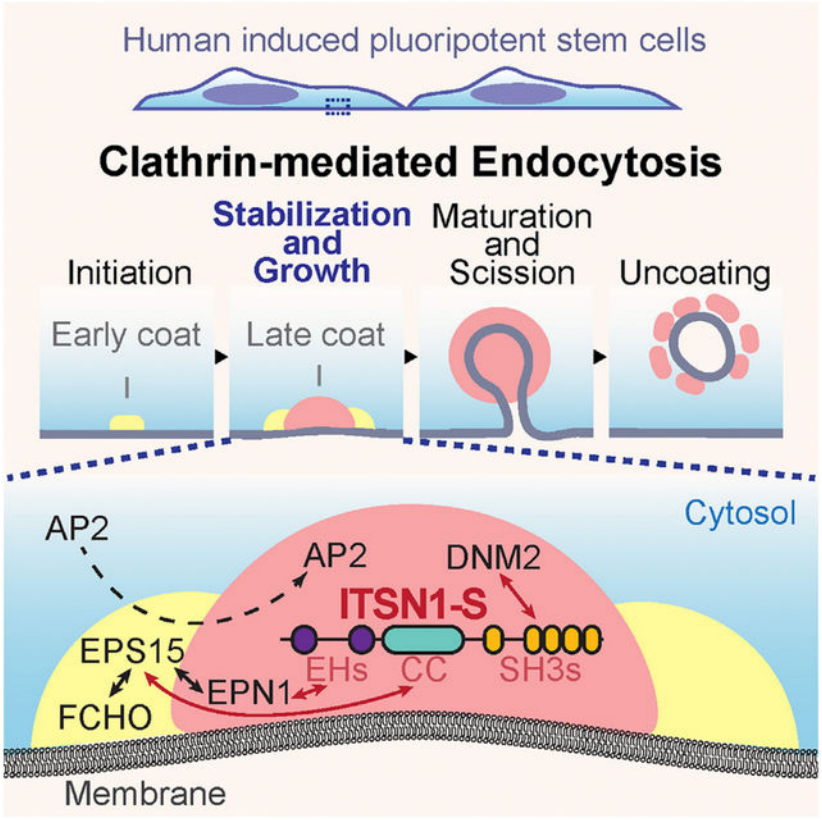

INTRODUCTION

Clathrin-mediated endocytosis (CME) is an essential process in eukaryotes that regulates cell signaling and mediates nutrient uptake, with over 60 proteins involved.[1–3] However, how endocytic protein recruitment is coordinated in time and space is not fully understood.

The CME process begins with initiation, which is followed by site stabilization, growth, maturation (when the coat protein accumulation plateaus), and then vesicle scission and uncoating (Figure 1A).[3,4] In the past decade, our understanding of the molecular mechanism of CME site initiation has improved significantly thanks to studies from multiple research groups. Recent studies suggest that the endocytic pioneer proteins EPS15[5] and FCHOs[6–8] might form liquid-like condensates on the plasma membrane.[9] Previous work suggests that the AP2 complex, the main CME cargo adaptor, is recruited to and activated at nascent CME sites through transient interactions with EPS15 and FCHO.[7,8,10,11] Combining knowledge of the ultrastructural organization of endocytic proteins from super-resolution imaging[12] and evidence of liquid condensate formation, a two-phase CME protein network assembly model has been proposed recently.[13] This model suggests that, subsequent to CME site initiation, which is proposed to involve the first liquid-liquid phase separation event, a second liquid-liquid phase separation event occurs, involving epsins and PICALM. As a result, a protein network at the center of the initial condensate forms and grows. This second

protein network contributes to CME site stabilization and growth by outcompeting EPS15 for binding to the cargo-bound AP2 complex[10,13,14] (Figure 1A). However, the molecular mechanism underlying the formation of this second phase and how the two putative phases are connected remains to be determined.

Intersectin1 (ITSN1) is a multivalent scaffold protein known to interact with multiple endocytic proteins.[6,16] ITSN1 has two main isoforms: a short, 140 kDa, universally expressed isoform, ITSN1-S, and a long, 200 kDa, neuron-specific isoform, ITSN1-L.[16–18] ITSN1's interactions implicate it as a key protein functioning at the nexus of initiation components (EPS15 and FCHO2) and the centrally localized proteins (CALM and epsins).[19,20] A knockdown screen involving 67 CME proteins suggested that ITSN1 might participate in CME site stabilization.[21] The combined evidence identifies ITSN1 as a candidate to form connections within CME protein networks and bridge putative liquid phases.

In contrast to a proposed role in CME site stabilization, ITSN1 has also been proposed to be a CME site initiation complex member because, when overexpressed, it arrives at CME sites simultaneously with EPS15 and FCHO, prior to the arrival of clathrin and AP2.[6] This latter proposal raises questions about whether ITSN1's true function is in CME site initiation or stabilization. Overexpressed proteins often display altered dynamics and functions[22,23]; however, the timing of endogenously expressed ITSN1's arrival and its potential role in CME site initiation have not been fully characterized.

In this study, through the combination of genome editing, live-cell imaging, high-throughput computational analysis, and a mitochondrion relocalization assay, we demonstrate that ITSN1-S plays a crucial role in CME site stabilization and growth by establishing an interaction network that interconnects endocytic proteins that arrive at different stages of CME and that localize to different spatial zones within CME sites.

RESULTS

ITSN1 is recruited during CME site stabilization and growth

Previous studies have shown that recruitment of the AP2 adaptor complex to CME sites occurs shortly after CME site initiation,[6,14] a process that some studies suggest is facilitated by liquid condensate formation on the plasma membrane by endocytic pioneer proteins, including EPS15 and FCHO.[6,13] While DNM2 is well known for its crucial role in vesicle scission during the final step of CME, our genome-edited DNM2-TagGFP2 faithfully reports its recruitment to CME sites in two phases: low-level recruitment during the assembly stage followed by a short burst of high-level recruitment during the late stage of CME.[15,22,24] Thus, the AP2M1-TagGFP-T and DNM2-TagGFP2 genome-edited human induced pluripotent stem cells (hiPSCs) used in our earlier studies can be used to elucidate the progression of various CME stages with a temporal resolution of seconds.

Although ITSN1 has been proposed to arrive at CME sites with the initiation proteins EPS15 and FCHOs,[6] knocking it down resulted in an increased rate of CME site initiation and a decreased rate of CME site maturation.[21] To determine the specific stage of CME at

which ITSN1 functions, we first investigated the timing of its recruitment. We transiently expressed HaloTag-ITSN1-S in genome-edited cells (AP2-TagRFP-T, DNM2-TagGFP2) through plasmid transfection. Although we observed co-localization of ITSN1 with AP2 and DNM2 on the plasma membrane, indicative of its recruitment to CME sites, CME dynamics in ITSN1-overexpressing cells markedly differed from adjacent control cells without ITSN1 overexpression (Figure S1A). This observation indicates that ITSN1 overexpression perturbs CME and should be avoided when studying its recruitment dynamics.

Therefore, to investigate ITSN1 recruitment timing in a close-to-native context, we generated a genome-edited AP2-TagRFP-T, mEGFP-ITSN1 hiPSC line (Figure 1B and S1B). Endogenously tagged ITSN1 was mainly expressed as the short splicing isoform in hiPSCs (Figure S1B) and, as expected, was recruited without obviously perturbing CME dynamics (Figure S1C). We observed that ITSN1 is recruited to CME sites either concurrently with AP2 or shortly thereafter (within 10 s); however, it is occasionally recruited significantly later than AP2 (more than 10 s) (Figure 1C).

To comprehensively investigate the spatiotemporal dynamics of ITSN1 at CME sites, we applied principal-component analysis (PCA) clustering to the AP2-positive sites computationally tracked by the cmeAnalysis program[25] in time-lapse images of genome-edited cells expressing tagged AP2 and ITSN1. Through analysis of 64,153 total AP2 tracks, 11,001 (17.15%), 26,684 (41.59%), 2,420 (3.77%), 16,072 (25.05%), and 7,976 (12.43%) tracks were classified into five clusters, clusters 0–4, respectively (Figure 2A). Structures in clusters 0 and 2 have very low AP2 intensity and consist of very-short-lived events (AP2 lifetimes are 3.0 ± 0.0 s for both clusters; Figures 2B, S2A, and S2B). These structures might represent transient coat fragments that fail to nucleate into CME sites.[25,26] The structures in clusters 1 and 3 also have low AP2 intensity but slightly higher than in clusters 0 and 2, and they are slightly longer lived (AP2 lifetimes: 8.1 ± 5.8 and 12.5 ± 10.8 s, respectively; Figures 2B, S2A, and S2B). These short-lived structures might represent abortive events where the initiated CME sites fail to grow and mature into clathrin-coated pits or vesicle visitors to the total internal reflection fluorescence (TIRF) field.[21,25] Cluster 4 sites are characterized by high AP2 intensity and are relatively long lived (AP2 lifetime: 62.7 ± 36.1 s) and move more slowly in the x and y axes than the sites in clusters 0–3 (very short-lived and short-lived tracks) (Figures 2B, S2A, and S2B), indicating that these structures, with higher CME adaptor content, interact more stably with the plasma membrane. Tracks with lifetimes longer than 20 s have been considered valid CME events.[1,27,28] Combining the AP2 intensity, lifetime, and lateral movement information, we propose that cluster 4 represents authentic CME events.[21,25,27] Enrichment of CME sites with high ITSN1 levels in this cluster (Figures 2B, S2A, S2C, and S2D) suggests an important role for ITSN1 in successful CME.

We detected a small population of events with a higher rate of AP2 intensity increase (>20 a.u. per second) across all clusters, particularly in clusters 3 and 4 (Figure S2E). These events most likely are “visitors,” where clathrin-coated vesicles rapidly move into the imaging field.[25,27] We were not able to filter out this population using our PCA clustering method; however, we observed that these events are enriched in the 0- to 30-s AP2 lifetime cohort in cluster 4 (long-lived tracks) (Figure S2E). Therefore, we named this cohort “fast

events," which may contain both CME events and vesicle visitors, to distinguish it from the rest of cluster 4 events (Figures 2C and S2E). We further grouped the remaining cluster 4 events based on their lifetimes into "standard CME" (30–110 s) and "slow CME" (110–240 s), where we began to observe a noticeable plateau stage, indicating that events in this cohort require extra maturation and/or invagination time (Figures 2C and S2C). In these CME events, AP2 recruitment rates are relatively consistent regardless of their lifetime, and longer assembly times are needed to recruit more AP2 (Figures 2C and S2C). This observation is consistent with others showing that amounts of proteins recruited to a CME site and lifetime are correlated.[8]

Moreover, we observed that cluster 4 (long-lived) tracks with longer AP2 lifetimes recruit higher amounts of ITSN1 (Figures 2C, S2A, and S2C), consistent with a high correlation between ITSN1 and AP2 recruitment levels in standard and slow CME events (Figure 2D). To study the potential function of ITSN1 in CME, we further analyzed the timing of ITSN1 recruitment to CME sites in standard and slow CME events within cluster 4 (long-lived tracks). To compare AP2 and ITSN1 recruitment dynamics, which were detected through two different fluorescent protein tags and using different imaging parameters, we normalized their fluorescence intensities and averaged events that fell into narrow lifetime windows to minimize averaging artifacts. Regardless to which protein's signal initiation we aligned (as time 0), in both standard and slow CME events containing at least 5 consecutive frames (5 s) of ITSN1 detection, we observed that ITSN1 and AP2 signals increase above background levels at approximately the same time, but ITSN1 reaches a plateau several seconds before AP2 (Figures 2E and S2F). We did not observe significant recruitment of ITSN1 prior to the detection of AP2 (low or undetectable ITSN1 intensity before time 0 in Figures 2E and S2F). These observations suggest a potential role for ITSN1 during CME site stabilization and growth rather than in initiation.

To further analyze the spatiotemporal dynamics of ITSN1 at CME sites, we compared the recruitment dynamics of endogenously tagged mEGFP-ITSN1 to endogenously tagged DNM2-tagGFP2, whose dynamics and functions in CME are better studied. DNM2 is recruited to CME sites in two stages. Early- to mid-stage DNM2, arriving at low levels, has potential roles in the stabilization and maturation of CME sites, while late-stage DNM2 performs the canonical membrane scission function.[25,28] We performed a computational analysis of AP2 tracks in AP2M1-TagGFP-T, mEGFP-ITSN1, and AP2M1-TagGFP-T, DNM2-TagGFP2 genome-edited cells (Figure S3A), collected from live-cell imaging performed on the same days under the same imaging settings using methods similar to those shown in Figure 2 (Figures 3A, 3B, and S3B–S3I). As reported previously,[15] AP2 tracks detected from AP2M1 and DNM2 genome-edited cells were classified into five clusters, with cluster 4 representing authentic, DNM2-positive CME events (Figures 3B, S3C, S3E, S3G, and S3I).

To estimate the total number of ITSN1 molecules recruited to each CME site, we compared the maximum intensities of ITSN1 to DNM2 in standard and slow CME tracks containing at least 5 consecutive frames of ITSN1 or DNM2 detection. The peak intensity of ITSN1 was about half that of DNM2 (137.79 ± 104.46 and 284.16 ± 251.91 a.u., respectively) (Figure 3C). Considering the similar brightness of mEGFP and TagGFP2 (1:1.05)[29] and that the

number of DNM2 molecules peaks at an average of 35–50 molecules,[30,31] we estimate that the number of ITSN1 molecules during CME peaks at one to two dozen on average.

Next, we compared the arrival timing of ITSN1 and DNM2 to CME sites. We detected ITSN1 or DNM2 signals prior to AP2 in only 18.47% and 16.37% of tracks, respectively (Figure 3D). Also, we did not observe higher ITSN1 intensity compared to DNM2 prior to AP2 detection in different cohorts of cluster 4 (long-lived) events (Figure 3E). There is no evidence for the recruitment of DNM2 at the initiation of CME sites, to our knowledge. Therefore, these data indicate that it is unlikely that ITSN1 is recruited to CME sites at the initiation stage, before AP2, in most CME events.

To summarize, the early- to mid-stage arrival timing of endogenously expressed ITSN1, coupled with the high correlation between ITSN1 and AP2 intensity at CME sites, is more consistent with a role for ITSN1 in CME site stabilization and growth than in site initiation.

ITSN1 promotes CME site stabilization and growth

To investigate ITSN1 function in CME, we conducted knockdown experiments using transiently expressed shRNAs targeting ITSN1. Each of two different shRNAs resulted in a pronounced reduction of ITSN1 expression (Figure S4A). Our studies used a combination of the two shRNAs for ITSN1 knockdown (KD) in genome-edited cells expressing fluorescent protein-tagged AP2 and DNM2. Kymograph analysis revealed a striking reduction in low-level DNM2 recruitment during the early to middle stages of CME in ITSN1 KD cells but not in the rapid, pronounced high-level recruitment late in CME (Figure 4A).

To compare CME dynamics in the control (scrambled shRNA) and ITSN1 KD cells in an unbiased, high-throughput manner, we performed computational analysis of AP2 tracks in AP2M1-TagGFP-T and DNM2-TagGFP2 genome-edited cells. Similar to the previous analysis, AP2 tracks detected from live-cell imaging of uncropped imaging areas, which contained a mixed population of untransfected cells and cells expressing either scrambled (control) or ITSN1-targeting shRNAs, were classified into five clusters, with cluster 4 representing DNM2-positive CME events (Figures S4B and S4C). Comparison of the distribution of AP2 tracks in these clusters within cropped imaging areas containing control and ITSN1 KD cells (Figure S4D) showed a pronounced reduction in the fraction of events grouped in cluster 4 (long-lived tracks), the authentic CME events, and increased fractions of events classified into clusters 3 (short-lived tracks) (Figures 4B and S4D). Additionally, there was an increase in the total number of events, which did not correlate with a detectable decrease in the fraction of events classified into cluster 4, suggesting that, in the ITSN1 KD cells, there may be more small AP2 clusters and/or events that fail to fully grow and mature (Figure 4B). These data are consistent with the increased initiation density detected in ITSN1 KD cells in a previous large-scale study.[21]

Furthermore, when comparing the recruitment dynamics of DNM2 and AP2 at CME sites (cluster 4), we observed reduced DNM2 and AP2 recruitment in the long-lifetime cohorts (≥90s) (Figures 4C and S4E). In contrast, the short-lifetime cohort (<90s) showed only moderately reduced recruitment of DNM2 during the early to middle stages, with no noticeable change in the late stage (Figure 4C). These findings suggest that a high level

of ITSN1 is particularly crucial for the efficient recruitment of endocytic proteins to long-lifetime CME sites, typically characterized by the recruitment of higher levels of endocytic proteins (Figures 2C and S3E).

Moreover, in ITSN1 KD cells, we observed that CME lifetime, coat assembly time, and maturation time were considerably longer (44.99 ± 25.34 vs. 40.44 ± 26.62, 35.01 ± 21.49 vs. 33.00 ± 21.58, and 9.98 ± 14.31 vs. 7.44 ± 13.11 s, respectively) (Figure 4D). DNM2 intensities at CME sites were lower, and DNM2 lateral movement was increased (Figure 4E). However, AP2 intensity and lateral movement were essentially unchanged within the total CME populations (cluster 4) (Figure S4F) but significantly changed only in the long-lifetime cohort (≥90s) (Figure 4F), establishing that DNM2 recruitment to and stabilization at CME sites are more sensitive to ITSN1 recruitment levels.

Together, these results indicate that ITSN1 plays crucial roles in CME site stabilization, growth, and maturation, particularly through early- to middle-stage DNM2 recruitment to, and stabilization at, CME sites.

ITSN1-S is sufficient to coalesce multiple endocytic proteins into puncta

To define the CME protein interaction network centered around ITSN1, we artificially relocated ITSN1 to the mitochondrial outer membrane by ectopically expressing ITSN1 conjugated to the Tom70 mitochondrion-targeting peptide.

This relocalization was sufficient to recruit multiple endocytic proteins, including EPS15, FCHO2, AP2M1, DNM2, and EPN1 (epsin1), to mitochondria and to coalesce them into puncta (Figure 5). These proteins exhibited high molecule exchange rates within the puncta, as demonstrated by fluorescence recovery after photobleaching assay. Both DNM2 and AP2 recover to approximately 60% intensity in less than 1 min (Figures S5A and S5B).

EPS15 and its yeast homolog, Ede1, can form condensates when overexpressed.[9,32] To test whether the proteins assembled around relocated ITSN1-S are distinct in composition from those present in EPS15-induced condensates, we artificially targeted EPS15 to mitochondria using the same strategy. Indeed, EPS15 forms puncta that contain FCHO2, AP2, and EPN1. However, we did not detect DNM2 in the mito-EPS15 puncta (Figure S5C). This result indicates that mito-ITSN1-S assembles puncta containing components beyond those present in the EPS15-FCHO-containing puncta.

Moreover, when we co-expressed mito-ITSN1-S and mito-EPS15 and examined their localization at high resolution, we observed that these proteins localize to the same puncta but occupy distinct regions within the puncta (Figure S5D). This observation further supports the notion that ITSN1 is centered within a protein network distinct in composition from that present in the EPS15-containing initiation condensate.

These data are consistent with the hypothesis that ITSN1 organizes a distinct protein interaction network and forms a bridge with the EPS15 interaction network, which functions in the initiation of CME sites, and that ITSN1 is responsible for the stable recruitment of proteins such as DNM2 that participate in later stages of CME.

ITSN1's different domains play distinct roles in establishing its interaction network

ITSN1 is a multidomain scaffold protein, with its short isoform containing two EH domains, a coiled-coil domain, and five SH3 domains.[17] The Eps15 homology (EH) domains are known to interact with asparagine-proline-phenylalanine (NPF) motif-containing proteins, including EPN1[20,33]; the coiled-coil (CC) domain is crucial for ITSN1 oligomerization and its interaction with other CC domain-containing proteins, such as EPS15[20]; and the five SH3 domains interact with proteins containing proline-rich domains (PRDs), including DNM2[20,34,35] (Figure 6A). To dissect the roles of ITSN1's different domains in establishing its interaction network, we expressed various truncated forms of ITSN1-S (Figure 6A) in the ITSN1 knockout (KO) cells. The ITSN1 KO cells were generated from the AP-TagRFP-T, mEGFP-ITSN1 cells using CRISPR-Cas9 genome editing, and GFP-negative cells were selected and pooled by the flow cytometry.

The CC and EH domains are both crucial for ITSN1 recruitment to CME sites (Figure 6B). Mutants lacking either the CC or EH domains could still form puncta when artificially targeted to mitochondria (Figure S6A). However, the CCΔ mutant did not recruit the CME initiation components EPS15 and FCHO2 or AP2M1. The CC domain of ITSN1 is known to interact with the CC domain of EPS15,[20] and ITSN1 dimerization through its CC domain may potentially strengthen this interaction through increased multivalency. Our observations suggest that ITSN1's recruitment to the initiation site that contains EPS15 and FCHO2 is primarily mediated through its CC domain (Figure 6C).

The mitochondrion relocalization assay also revealed that CCΔ or EHΔ mutants of ITSN1-S can still interact with EPN1. However, an EHΔCCΔ mutant lacking both the CC and EH domains did not recruit EPN1 to the ITSN1-S-containing puncta (Figure 6C). This result suggests that the interaction between ITSN1-S and EPN1 is mediated redundantly through ITSN1's CC and EH domains. The most likely explanation for this observation is that ITSN1's EH domains can interact with EPN1's NPF motif, while its CC domain mediates an indirect interaction with EPN1 through EPS15 (EPS15 contains EH domains that interact with EPN1's NPF motif[36]) and strengthen ITSN1-EPN1 interaction through increased multivalency.

Interestingly, the EHΔCCΔ mutant can still form puncta and recruit DNM2 (Figure S6B). This result supports the conclusion that ITSN1 interacts with DNM2 independent of EPS15/FCHO2 and EPN1.

In contrast, the SH3Δ mutant of ITSN1-S forms dimmer puncta when targeted to mitochondria (Figure S6A). The mito-ITSN1 SH3Δ puncta contain EPS15, FCHO2, EPN1, and AP2M1 (Figure S7) but do not contain detectable DNM2 (Figure 7A). This result suggests that ITSN1's SH3 domains are crucial for its interaction with PRD-containing proteins like DNM2 and that this interaction is important for ITSN1's ability to establish strong interaction networks.

The above observations are consistent with a model in which ITSN1 is recruited to nascent CME sites through its interaction with a complex network of endocytic proteins responsible for initiation. It has been suggested that these early endocytic proteins form a

condensate. We propose that, subsequent to CME site initiation, ITSN1 mediates a CME site stabilization step by nucleating and stabilizing a protein interaction network associated with, but distinct from, the initiation complex (Figure 7B). Recent data raise the intriguing possibility that both complexes might have properties of liquid condensates.[9,13]

DISCUSSION

In this study, we used genome editing to minimize perturbation of the recruitment dynamics of ITSN1 and redefined ITSN1's function, implicating it in CME site stabilization and growth rather than in initiation, which was its previously proposed role[6] (Figure 7B). Our results resolve a contradiction between the identification of ITSN1 as a part of the EPS15-FCHO-ITSN1 initiation complex, the observation that ITSN1 has a distinct localization pattern from EPS15 and FCHO at CME sites,[12] and ITSN1 KD phenotypes that differ from those of EPS15.[21] While depletion of EPS15 results in reduced rates of CME initiation events, we detected increased rates of short-lived, low-AP2-intensity events in ITSN1 KD cells (Figure 4B), a phenotype commonly associated with compensatory activities that trigger CME site initiation in cells where early-stage CME proteins, potentially functioning downstream of CME initiation (e.g., AP2 subunits, Dab2, NECAP1, Epsin2, and Hip1R), have been depleted.[21] Interestingly, a similar phenotype has been reported in FCHO knockdown cells in the same study,[21] suggesting a potential role for FCHO in later stages of CME, beyond initiation. Our study highlights the problems associated with overexpressing proteins of interest, especially those with multivalent interaction domains and prone to condensate formation upon overexpression. Overexpressing one or more endocytic protein can lead to their premature recruitment or delayed disassociation from CME sites, consequently over-stabilizing CME sites.[21]

Here, we showed that ITSN1 interacts with multiple endocytic proteins and contributes to their efficient recruitment to CME sites (Figures 4, 5, 6, and 7). It is interesting to note that the late-stage recruitment of DNM2 is not significantly affected by ITSN1 KD, while the low-level, early- to middle-stage CME site recruitment of DNM2 is dependent on ITSN1 (Figures 4A and 4C). This result supports the model where DNM2 plays roles during multiple stages of CME[37] and that its recruitment at different stages is regulated through independent mechanisms. Proteins that contain both SH3 and Bin/amphiphysin/Rvs domains, such as amphiphysin, have been proposed to work cooperatively with DNM2 to be recruited to the highly curved clathrin-coated vesicle neck.[37,38] Additionally, DNM2 itself has been suggested to act as a curvature sensor.[39] While DNM2's role in scission at the late stage of CME has been conclusively demonstrated and extensively studied, its function in the earlier stages remains understudied and is not fully understood.[28,40] It has been suggested previously that ITSN1 might recruit early-stage DNM2, although no direct evidence was provided.[37] Based on our findings, we hypothesize that early-stage DNM2, together with other PRD-containing proteins and ITSN1, contribute to CME site stabilization and growth[28] by formation of a second liquid condensate after the initiation condensate through PRD-SH3 multivalent interactions (Figure 7B).

To our surprise, although we observed dissociation of ITSN1 from CME sites before AP2 (Figures 1C and 2E), we detected longer CME site maturation times in the ITSN1 KD cells

(Figure 4D), suggesting a potential role for ITSN1 in the later stages of CME. DNM and actin are proposed to function in CME site maturation, invagination, and scission.[15,30,41] Besides its interaction with dynamin, ITSN1 is known to interact with actin assembly regulators such as neuronal Wiskott-Aldrich syndrome protein (N-WASP) and WAS/WASL-interacting protein (WIP).[38,42] Additionally, ITSN1 binds to endophilin and has been implicated in clathrin-coated vesicle uncoating in synapses.[43] Thus, it would be intriguing to further investigate ITSN1's role in the late stages of CME or under conditions of enhanced dependence on actin assembly in future studies.

Our computational analysis showed that, in ITSN1 KD cells, the CME sites with the highest AP2 intensity are absent from the population, suggesting that ITSN1 may be particularly important when a high level of AP2-mediated cargo uptake is required (Figures 4C and 4F). This putative cargo/signal-specific ITSN1 function may be an important component of its normal function and important for certain disease states, as growing evidence links mutations in ITSN1 to increased autism risk, and ITSN1 is suggested to play an important role in neuronal development.[44–47]

In summary, in this study, we provided evidence that ITSN1 promotes CME site stabilization and growth. Our results are consistent with the recently proposed model where CME site formation, stabilization, and growth involve multiple distinct but interacting protein liquid condensates and offer insights into how ITSN1 might contribute to the organization of such a multi-condensate system by promoting the stable assembly of the ITSN1-centered condensate and bridging it to an earlier-arriving initiation phase condensate composed of EPS15 and FCHO proteins (Figure 7B).

Limitations of the study

In this study, we could not gather sufficient evidence that the mito-ITSN1-S-containing puncta are liquid condensates. However, even if we could have demonstrated condensate formation, the uncontrolled expression of mito-ITSN1 prevented us from reconstituting an ITSN1-DNM2 interaction network with the same protein stoichiometry present at natural CME sites. Therefore, despite providing further insights into the previously proposed model where multiple, distinct liquid condensates form at CME sites,[13] additional evidence is required to determine whether and how liquid condensates contribute to the assembly of different functional subdomains of CME sites.

ITSN1 has a homolog, ITSN2, that shares the same domain structures with ITSN1. Due to the low expression of ITSN2 in iPSCs, we were not able to genome-edit ITSN2 and compare its dynamics and function to those of ITSN1. However, in the future, it will be important to explore the function of ITSN2 in a cell type in which it is expressed at higher levels.

As CME is an essential process, we anticipate that genetic modifications causing severe defects in CME would lead to cell death or activate compensatory pathways to support cell survival. Indeed, we observed a very small population of ITSN1-targeting shRNA-transfected cells when we observed the cells for a longer time after transfection, indicating reduced cell viability with prolonged ITSN1 KD. Consequently, we performed imaging in cells experiencing only partial ITSN1 KD (Figure S4A) and observed some compensatory

phenotypes, such as increased total AP2 track numbers (Figure 4B). We believe that detecting severe CME defects is likely to be technically more challenging in iPSCs compared to cancer cell lines, where cell death pathways are often suppressed. It has been reported that about 40% of ITSN1 KO or ITSN1/ITSN2 double KO mice die prenatally.[48,49] Overall, we believe that ITSN is playing a vital role but were limited to observing partial KD phenotypes due to the apparent severity of high-efficiency KD.

Although we were able to implicate specific ITSN1 domains in the specific functions (Figures 6 and 7), complexity and redundancy in functions and interactions prevented us from pinpointing the domains of ITSN1 that are responsible for its direct interactions with EPN1, FCHO2, and AP2. Additionally, whether EPN1 exists in the same interaction network with ITSN1 or forms a distinct protein complex/liquid condensate requires further investigation.

Our PCA-based clustering method is a powerful tool for unbiased and quantitative detection of various parameters of CME events. However, since clustering is based on features extracted from two different CME proteins (AP2M1 and ITSN1 or DNM2), the choice of the second protein can significantly affect the differentiation between clusters 0 and 2 (very short-lived tracks) as well as clusters 1 and 3 (short-lived tracks) (note the changes in the percentiles of these clusters when we used ITSN1 vs. DNM2 as the second CME protein, as shown in Figure 3A vs. Figure 3B). Additionally, we were unable to distinguish vesicle visitors from other CME-related structures using our current methods (Figure S2E). These limitations will need to be addressed in future studies.

RESOURCE AVAILABILITY

Lead contact

Requests for further information, data, and materials should directed to and will be fulfilled by the lead contact, David G. Drubin (drubin@berkeley.edu).

Materials availability

Plasmids and cell lines generated in this study will be available upon request.

Data and code availability

Raw data and original code have been deposited at Zenodo. DOIs are listed in the key resources table. They are publicly available as of the date of publication. Any additional information required to reanalyze the data reported in this paper is available from the lead contact upon request.

STAR★METHODS

EXPERIMENTAL MODEL AND STUDY PARTICIPANT DETAILS

The WTC hiPSC parental cell line (male, Coriell Cat. # GM25256) was obtained from the Bruce Conklin Lab at UCSF. All the cell lines used in the study were generated by genome editing of the WTC hiPSC line by the authors. AP2, DNM2, and AP2, ITSN1

genome-edited cell lines used in this study were verified by genomic DNA purification, Sanger sequencing and western blotting. All the cell lines used in this study tested negative for mycoplasma contamination by PCR and authenticated by the University of California, Berkeley Cell Culture Facility using short tandem repeat (STR) analysis. The hiPSCs were cultured on Matrigel (hESC-Qualified Matrix, Sigma-Aldrich, Cat# CLS354277) in StemFlex medium (Thermo Fisher Scientific, Cat# A3349401) with Penicillin/Streptomycin in 37°C, 5% CO2. Cultures were passaged with Gentle Cell Dissociation reagent (StemCell Technologies, Cat#: 100–0485) twice every week.

METHOD DETAILS

Cell culture—The WTC hiPSC line was sourced from the Bruce Conklin Lab at the University of California, San Francisco. The hiPSCs were grown on Corning Matrigel hESC-Qualified Matrix (Sigma-Aldrich, Cat# CLS354277) in StemFlex medium (Thermo Fisher Scientific, Cat# A3349401) supplemented with Penicillin/Streptomycin at 37°C with 5% CO2. Passaging of cell cultures was conducted biweekly using Gentle Cell Dissociation Reagent (StemCell Technologies, Cat# 100–0485).

Genome editing—The Cas9-sgRNA complex electroporation method was used to knock in mEGFP at the 5′ of the ITSN1 gene in AP2M1-tagRFP-T genome-edited hiPSCs. *S. pyogenes* NLS-Cas9 was purchased from the University of California Berkeley QB3 MacroLab. sgRNA targets AGGTGTTGGAAACTGAGCCA was purchased from Synthego. NEBuilder HiFi DNA Assembly Master Mix (New England Biolabs, Cat# E2621S) was used to construct the donor plasmid containing 450 bp ITSN1 5′ homology arm including start codon, mEGFP, a linker sequence: AAG TCC GGA GGT ACT CAG ATC TCG AGG, and 447bp ITSN1 3′ homology arm sequence. Following electroporation (Lonza, Cat#: VPH-5012) of the Cas9-sgRNA complex and the donor plasmid, mEGFP-positive hiPSCs were individually sorted into Matrigel-coated 96-well plates using a BD Bioscience Influx sorter (BD Bioscience) three days later. The confirmation of clones was carried out through PCR and Sanger sequencing of the genomic DNA surrounding the insertion site. Both alleles of ITSN1 were tagged with mEGFP.

The Cas9-sgRNA complex electroporation method was used to knockout ITSN1 in the AP2M1-tagRFP-T, mEGFP-ITSN1 genome-edited hiPSCs. sgRNA targets GAAGTTCGAGGGCGACACCC was purchased from Synthego. mEGFP-negative and tagRFP-T-positive hiPSCs were pooled into Matrigel-coated plates using a BD Bioscience Influx sorter (BD Bioscience), three days after electroporation (Lonza, Cat#: VPH-5012) of the Cas9-sgRNA complex. Verification of the absence of mEGFP-ITSN1 expression was conducted through fluorescence microscopy.

Lysate preparation and western blotting—Each iPSC lysate was prepared from one well of a 6-well plate. Cells were washed in PBS, incubated in 200ul lysis buffer (50mM HEPES pH 7.4, 150mM NaCl, 1mM MgCl2, 1% NP40, phosSTOP (Roche, Cat# 4906845001), protease inhibitor (Roche, Cat# 1183617001)) for 15 min at room temperature. After collecting the supernatant, it was centrifuged at 4°C and 13,000rpm for

15 min. The lysate was combined with Laemmli reducing buffer (5% β-mercaptoethanol) and boiled for 10 min for Western blot analysis.

PageRuler Plus Prestained Protein Ladder (Thermo Fisher Scientific, Cat# 26619) and cell lysate samples were loaded onto a polyacrylamide gel for SDS-PAGE and transferred onto nitrocellulose membrane via overnight wet transfer. Blots were blocked with 5% milk in TBS (Tris-buffered saline) and incubated with primary antibody at 4°C overnight. For primary antibody blotting, anti-(CGY)FP (1:2000 dilution in 1% milk in TBS, Evrogen, Cat# AB121) and anti-GAPDH (1:10000 in TBST, Abcam ab9485) were used. Finally, blots were incubated with IRDye 800CW secondary antibodies (Licor, Cat# 926–32211 and Cat# 926–32210) diluted 1:10,000 in TBST containing 5% milk for 1 h at room temperature and imaged on the LICOR Odyssey DLx imager.

TIRF live-cell imaging—Two days prior to imaging, human induced pluripotent stem cells (hiPSCs) were plated onto Matrigel-coated 8-well chambered cover glasses (Cellvis, Cat# C8–1.5H-N). If plasmid transfection was required (ITSN1 overexpression or knockdown), during cell plating, 300ng of plasmid was transfected using Lipofectamine Stem Transfection Reagent (Thermo Fisher Scientific, Cat# STEM00001) in 150μL Opti MEM, along with 10μM ROCK inhibitor Y-27632 (Chemdea, Cat# CD0141) for each well. Four hours post-transfection, 150μL StemFlex medium with 10μM ROCK inhibitor was added to each well, followed by a switch to StemFlex medium 24 h after transfection. For HaloTag-ITSN1 imaging, before imaging, cells were incubated in StemFlex medium with 100 mM JF635-HaloTag ligand for 1 h. Unbound ligands were removed through three washes, each involving a 5-min incubation in prewarmed StemFlex medium. Imaging was conducted using a Nikon Ti-2 inverted microscope equipped with 60x total internal reflection fluorescence (TIRF) optics and a sCMOS camera (Hamamatsu). Cells were maintained at 37°C throughout the imaging process using a stagetop incubator (OKO Lab) in StemFlex medium supplemented with 10 mM HEPES. Nikon Elements software was utilized for image acquisition, capturing channels sequentially at a 1-s intervals with a 300ms exposure time over a 4-min duration.

TIRF image processing—Three generalized processing steps were applied to cluster AP2-positive events: track feature abstraction, feature dimensionality reduction, and event clustering.

First, trajectories, delineated by fitted positions and intensities for individual AP2 positive events, were created using cmeAnalysis.[25] AP2-tagRFP-T served as the master channel for clathrin-mediated endocytosis in cmeAnalysis tracking experiments. DNM2-tagGFP2 or mEGFP-ITSN1 was used as a secondary channel.

Subsequently, within Python Jupyter notebooks, AP2 and ITSN1(or DNM2) tracks underwent decomposition into 28 dynamic features that characterized the events' positional changes and brightness variations. These features include AP2 track lifetime, maximum AP2 and ITSN1 (or DNM2) intensities, AP2 and ITSN1 (or DNM2) traveled displacement to distance ratios, maximum distance between AP2 and ITSN1 (or DNM2), AP2 and ITSN1 (or DNM2) mean displacements, time between AP2 and ITSN1 (or DNM2) peaks, average

AP2 and ITSN1 (or DNM2) intensity increase rates before the peak, average AP2 and ITSN1 (or DNM2) intensity increase rates after the peak, peak intensity difference between AP2 and ITSN1 (or DNM2), AP2 and ITSN1 (or DNM2) maximum intensity ratio, mean AP2 and ITSN1 (or DNM2) intensities, variation of AP2 and ITSN1 (or DNM2) intensities, skewness values of AP2 and ITSN1 (or DNM2) intensity, kurtosis values of AP2 and ITSN1 (or DNM2) intensity, number of ITSN1 (or DNM2) positive frames, maximum number of consecutive ITSN1 (or DNM2) positive frames, fraction of ITSN1 (or DNM2) positive frames, fraction of the frames before the AP2 peak, and fraction of the frames before the ITSN1 (or DNM2) peak. Each tracked event, once an arbitrary array of intensities and positions, was now a discrete vector of fixed length. Each track was mapped to discrete features to generalize the dynamics of heterogeneous tracked events into a set of interpretable coordinates.

Following feature abstraction, the output array is a 2-dimensional matrix with N rows (N tracked events) and M columns (M discrete features per track). These features were individually scaled to normal distributions to remove the variability in scale and dampen the effects of outliers. For instance, the ‘lifetime’ feature (AP2 lifetime) ranged from a few seconds to several minutes on a scale of seconds, whereas the ‘DNM2-peak fraction’ feature (where the DNM2 peak is located within one AP2 event) ranges from 0 to 1. Following feature re-scaling, these events, which each contain over thirty features, were projected to a lower-dimensional space via principal component analysis. The derived clusters were separated using a Gaussian Mixture Model and events were assigned to clusters based on their highest probability of identity to one cluster.

The resultant data underwent downstream analysis.

Comprehensive Jupyter notebook codes detailing each step are accessible at Zenodo: http://doi.org/10.5281/zenodo.13737779 as of the date of publication.

Confocal fluorescence imaging—Two days prior to fixation, hiPSCs were single-cell passaged onto Matrigel-coated 8-well chambered cover glasses (Cellvis, Cat# C8–1.5H-N). During cell plating, 300ng of plasmid was transfected using Lipofectamine Stem Transfection Reagent in 150μL Opti MEM, along with 10μM ROCK inhibitor Y-27632 (Chemdea, Cat# CD0141) for each well. Four hours post-transfection, 150μL StemFlex medium with 10μM ROCK inhibitor was added to each well, followed by a switch to StemFlex medium 24 h after transfection.

Before fixation, cells were incubated in StemFlex medium with 100 mM JF635-HaloTag ligand for 1 h, and unbound ligands were removed through three washes, each involving a 5-min incubation in prewarmed StemFlex medium. Subsequently, cells were fixed for 20 min in 4% (v/v) PFA (Electron Microscopy Sciences, Cat#: 15710) in PBS, followed by three 10-min washes in PBS.

For samples requiring antibody staining, a 20-min block was performed using blocking buffer [3% (w/v) BSA and 0.1% (w/v) Saponin in PBS]. Primary antibody immunostaining was performed overnight at 4°C. The next day, samples underwent three 10-min washes in

washing buffer (0.1x blocking buffer in PBS). Secondary antibody incubation took place for 30 min at room temperature, followed by three 10-min washes in washing buffer and three 10-min washes in PBS.

Fixed cell samples were imaged on a Zeiss LSM 900 inverted microscope equipped with a Zeiss 60x objective (NA1.4) and an Airyscan 2 detector using Multiplex 4Y line scanning mode. Image acquisition and processing were performed using the ZEN 3.1 system. Channels were acquired sequentially, and images underwent 3D Airyscan processing.

FRAP assay—Movies for FRAP analysis were acquired using a Zeiss 60x objective (NA1.4) on a Zeiss LSM900 microscope in the point-scan confocal imaging mode. For acquisition, the pinhole size and laser speed were set to max and the optimal frame size was selected. Images were acquired every 2 s and photobleaching was conducted after a 10 frame pre-bleach period. To ensure that the photobleached puncta stayed in focus, we imaged a mito-HaloTag-ITSN1 (labeled by JF635-HaloTag ligand[53]) reference protein that localizes to the puncta but does not photobleach. All imaging was conducted at 37°C.

For FRAP analysis, the acquired movies were first background subtracted and subjected to photobleach correction using the ImageJ photobleach correction function (exponential fit). For all puncta analyzed, the reference puncta of the acquired movies were tracked using the ImageJ plug-in suite PatchTrackingTools,[54,55] and the intensity change of the bleached channel at the reference puncta location was monitored. The obtained intensity values were pooled by first normalizing every intensity value of a trace to the first measured intensity value, and then to then to the average intensity value over the prebleach period. After normalization, these traces were pooled, and the average trace was plotted along with the standard deviation for each time point. Importantly, in each case, we bleached the entire puncta, so whether the recovery is diffusion or reaction-limited is unclear. Plots were generated in a python notebook using the seaborn, numpy, and pandas packages. The notebook is accessible at Zenodo: http://doi.org/10.5281/zenodo.13737779 as of the date of publication.

QUANTIFICATION AND STATISTICAL ANALYSIS

Excel, MATLAB and Python were used for quantification and statistical analysis. The statistical details of experiments can be found in each figure and its corresponding legend, where applicable.

Supplementary Material

Refer to Web version on PubMed Central for supplementary material.

ACKNOWLEDGMENTS

M.J. was funded by an American Heart Association postdoctoral fellowship (18POST34000029). D.G.D. was funded by NIH MIRA grant R35GM118149. pEGFPC1-EPSIN1 was a gift from Pietro De Camilli (Addgene plasmid 22228; RRID: Addgene_22228). The EPS15-EGFP (human) plasmid was a gift from the Taraska Lab at NIH. The EGFP-FCHO2 (mouse) plasmid was a gift from the McMahon Lab at the MRC Laboratory of Molecular Biology. The authors would like to thank Amy Yan and Yuang Song for their assistance with generating plasmids and genome-edited cell lines, Samantha L. Smith for assistance with cell culture during the revision of

this work, the Conklin Lab at UCSF for providing the WTC10 human iPSC line, the Lavis Lab at Janelia Research Campus for providing JF635 HaloTag ligand, the Xu Lab at UC Berkeley for providing the Tom20 antibody, the UC Berkeley QB3 MacroLab for purified *S. pyogenes* NLS-Cas9, the Luo Lab at UC Berkeley for sharing their electroporator, the Brar and Ünal Lab at UC Berkeley for sharing their LI-COR imager, and the UC Berkeley Cancer Research Laboratory Flow Cytometry Facility for iPSC sorting. The authors gratefully acknowledge the developers of the cmeAnalysis program and the Python packages employed in this study for generously providing their code on a free and open-source basis.

REFERENCES

1. Taylor MJ, Perrais D, and Merrifield CJ (2011). A high precision survey of the molecular dynamics of mammalian clathrin-mediated endocytosis. PLoS Biol. 9, e1000604. 10.1371/journal.pbio.1000604. [PubMed: 21445324]
2. Lu R, Drubin DG, and Sun Y (2016). Clathrin-mediated endocytosis in budding yeast at a glance. J. Cell Sci. 129, 1531–1536. 10.1242/jcs.182303. [PubMed: 27084361]
3. Kaksonen M, and Roux A (2018). Mechanisms of clathrin-mediated endocytosis. Nat. Rev. Mol. Cell Biol. 19, 313–326. 10.1038/nrm.2017.132. [PubMed: 29410531]
4. Mettlen M, Chen PH, Srinivasan S, Danuser G, and Schmid SL (2018). Regulation of Clathrin-Mediated Endocytosis. Annu. Rev. Biochem. 87, 871–896. 10.1146/annurev-biochem-062917-012644. [PubMed: 29661000]
5. Tebar F, Sorkina T, Sorkin A, Ericsson M, and Kirchhausen T (1996). Eps15 is a component of clathrin-coated pits and vesicles and is located at the rim of coated pits. J. Biol. Chem. 271, 28727–28730. 10.1074/jbc.271.46.28727. [PubMed: 8910509]
6. Henne WM, Boucrot E, Meinecke M, Evergren E, Vallis Y, Mittal R, and McMahon HT (2010). FCHo proteins are nucleators of Clathrin-Mediated endocytosis. Science 328, 1281–1284. 10.1126/science.1188462. [PubMed: 20448150]
7. Umasankar PK, Ma L, Thieman JR, Jha A, Doray B, Watkins SC, and Traub LM (2014). A clathrin coat assembly role for the muniscin protein central linker revealed by TALEN-mediated gene editing. Elife 3, e04137. 10.7554/eLife.04137. [PubMed: 25303365]
8. Lehmann M, Lukonin I, Noé F, Schmoranzer J, Clementi C, Loerke D, and Haucke V (2019). Nanoscale coupling of endocytic pit growth and stability. Sci. Adv. 5, 1–12. 10.1126/sciadv.aax5775.
9. Day KJ, Kago G, Wang L, Richter JB, Hayden CC, Lafer EM, and Stachowiak JC (2021). Liquid-like protein interactions catalyse assembly of endocytic vesicles. Nat. Cell Biol. 23, 366–376. 10.1038/s41556-021-00646-5. [PubMed: 33820972]
10. Ma L, Umasankar PK, Wrobel AG, Lymar A, McCoy AJ, Holkar SS, Jha A, Pradhan-Sundd T, Watkins SC, Owen DJ, and Traub LM (2016). Transient Fcho1/2•Eps15/R•AP-2 Nanoclusters Prime the AP-2 Clathrin Adaptor for Cargo Binding. Dev. Cell 37, 428–443. 10.1016/j.devcel.2016.05.003. [PubMed: 27237791]
11. Hollopeter G, Lange JJ, Zhang Y, Vu TN, Gu M, Ailion M, Lambie EJ, Slaughter BD, Unruh JR, Florens L, and Jorgensen EM (2014). The membrane-associated proteins FCHo and SGIP are allosteric activators of the AP2 clathrin adaptor complex. Elife 3, e03648. 10.7554/eLife.03648. [PubMed: 25303366]
12. Sochacki KA, Dickey AM, Strub MP, and Taraska JW (2017). Endocytic proteins are partitioned at the edge of the clathrin lattice in mammalian cells. Nat. Cell Biol. 19, 352–361. 10.1038/ncb3498. [PubMed: 28346440]
13. Witkowska A, and Haucke V (2021). Liquid-like protein assemblies initiate endocytosis. Nat. Cell Biol. 23, 301–302. 10.1038/s41556-021-00665-2. [PubMed: 33820974]
14. Zaccai NR, Kadlecova Z, Dickson VK, Korobchevskaya K, Kamenicky J, Kovtun O, Umasankar PK, Wrobel AG, Kaufman JGG, Gray SR, et al. (2022). FCHO controls AP2's initiating role in endocytosis through a PtdIns(4,5)P 2 -dependent switch. Sci. Adv. 8, eabn2018. 10.1126/sciadv.abn2018. [PubMed: 35486718]
15. Jin M, Shirazinejad C, Wang B, Yan A, Schöneberg J, Upadhyayula S, Xu K, and Drubin DG (2022). Branched actin networks are organized for asymmetric force production during clathrin-

mediated endocytosis in mammalian cells. Nat. Commun. 13, 3578. 10.1038/s41467-022-31207-5. [PubMed: 35732852]

16. Tsyba L, Nikolaienko O, Dergai O, Dergai M, Novokhatska O, Skrypkina I, and Rynditch A (2011). Intersectin multidomain adaptor proteins: Regulation of functional diversity. Gene 473, 67–75. 10.1016/j.gene.2010.11.016. [PubMed: 21145950]
17. Mintoo M, Rajagopalan V, and O'Bryan JP (2024). Intersectin - many facets of a scaffold protein. Biochem. Soc. Trans. 52, 1–13. 10.1042/BST20211241.
18. Herrero-Garcia E, and O'Bryan JP (2017). Intersectin scaffold proteins and their role in cell signaling and endocytosis. Biochim. Biophys. Acta. Mol. Cell Res. 1864, 23–30. 10.1016/j.bbamcr.2016.10.005. [PubMed: 27746143]
19. Wong KA, Wilson J, Russo A, Wang L, Okur MN, Wang X, Martin NP, Scappini E, Carnegie GK, and O'Bryan JP (2012). Intersectin (ITSN) family of scaffolds function as molecular hubs in protein interaction networks. PLoS One 7, e36023. 10.1371/journal.pone.0036023. [PubMed: 22558309]
20. Sengar AS, Wang W, Bishay J, Cohen S, and Egan SE (1999). The EH and SH3 domain Ese proteins regulate endocytosis by linking to dynamin and Eps15. EMBO J. 18, 1159–1171. 10.1093/emboj/18.5.1159. [PubMed: 10064583]
21. Bhave M, Mino RE, Wang X, Lee J, Grossman HM, Lakoduk AM, Danuser G, Schmid SL, and Mettlen M (2020). Functional characterization of 67 endocytic accessory proteins using multiparametric quantitative analysis of CCP dynamics. Proc. Natl. Acad. Sci. USA 117, 31591–31602. 10.1073/pnas.2020346117. [PubMed: 33257546]
22. Doyon JB, Zeitler B, Cheng J, Cheng AT, Cherone JM, Santiago Y, Lee AH, Vo TD, Doyon Y, Miller JC, et al. (2011). Rapid and efficient clathrin-mediated endocytosis revealed in genome-edited mammalian cells. Nat. Cell Biol. 13, 331–337. 10.1038/ncb2175. [PubMed: 21297641]
23. Gibson TJ, Seiler M, and Veitia RA (2013). The transience of transient overexpression. Nat. Methods 10, 715–721. 10.1038/nmeth.2534. [PubMed: 23900254]
24. Dambournet D, Sochacki KA, Cheng AT, Akamatsu M, Taraska JW, Hockemeyer D, and Drubin DG (2018). Genome-edited human stem cells expressing fluorescently labeled endocytic markers allow quantitative analysis of clathrin-mediated endocytosis during differentiation. J. Cell Biol. 217, 3301–3311. 10.1083/jcb.201710084. [PubMed: 29980624]
25. Aguet F, Antonescu CN, Mettlen M, Schmid SL, and Danuser G (2013). Advances in analysis of low signal-to-noise images link dynamin and AP2 to the functions of an endocytic checkpoint. Dev. Cell 26, 279–291. 10.1016/j.devcel.2013.06.019. [PubMed: 23891661]
26. Cocucci E, Aguet F, Boulant S, and Kirchhausen T (2012). The first five seconds in the life of a clathrin-coated pit. Cell 150, 495–507. 10.1016/j.cell.2012.05.047. [PubMed: 22863004]
27. Hong SH, Cortesio CL, and Drubin DG (2015). Machine-Learning-Based Analysis in Genome-Edited Cells Reveals the Efficiency of Clathrin-Mediated Endocytosis. Cell Rep. 12, 2121–2130. 10.1016/j.celrep.2015.08.048. [PubMed: 26387943]
28. Loerke D, Mettlen M, Yarar D, Jaqaman K, Jaqaman H, Danuser G, and Schmid SL (2009). Cargo and dynamin regulate clathrin-coated pit maturation. PLoS Biol. 7, e57. 10.1371/journal.pbio.1000057. [PubMed: 19296720]
29. Subach OM, Gundorov IS, Yoshimura M, Subach FV, Zhang J, Grüenwald D, Souslova EA, Chudakov DM, and Verkhusha VV (2008). Conversion of Red Fluorescent Protein into a Bright Blue Probe. Chem. Biol. 15, 1116–1124. 10.1016/j.chembiol.2008.08.006. [PubMed: 18940671]
30. Grassart A, Cheng AT, Hong SH, Zhang F, Zenzer N, Feng Y, Briner DM, Davis GD, Malkov D, and Drubin DG (2014). Actin and dynamin2 dynamics and interplay during clathrin-mediated endocytosis. J. Cell Biol. 205, 721–735. 10.1083/jcb.201403041. [PubMed: 24891602]
31. Cocucci E, Gaudin R, and Kirchhausen T (2014). Dynamin recruitment and membrane scission at the neck of a clathrin-coated pit. Mol. Biol. Cell 25, 3595–3609. 10.1091/mbc.E14-07-1240. [PubMed: 25232009]
32. Kozak M, and Kaksonen M (2022). Condensation of Ede1 promotes the initiation of endocytosis. Elife 11, e72865. 10.7554/eLife.72865. [PubMed: 35412456]

33. Yamabhai M, Hoffman NG, Hardison NL, McPherson PS, Castagnoli L, Cesareni G, and Kay BK (1998). Intersectin, a novel adaptor protein with two Eps15 homology and five Src homology 3 domains. J. Biol. Chem. 273, 31401–31407. 10.1074/jbc.273.47.31401. [PubMed: 9813051]
34. Knezevic I, Predescu D, Bardita C, Wang M, Sharma T, Keith B, Neamu R, Malik AB, and Predescu S (2011). Regulation of dynamin-2 assembly-disassembly and function through the SH3A domain of intersectin-1s. J. Cell Mol. Med. 15, 2364–2376. 10.1111/j.1582-4934.2010.01226.x. [PubMed: 21129155]
35. Okamoto M, Schoch S, and Südhof TC (1999). EHSH1/intersectin, a protein that contains EH and SH3 domains and binds to dynamin and SNAP-25. A protein connection between exocytosis and endocytosis? J. Biol. Chem. 274, 18446–18454. 10.1074/jbc.274.26.18446. [PubMed: 10373452]
36. Chen H, Fre S, Slepnev VI, Capua MR, Takei K, Butler MH, Di Fiore PP, and De Camilli P (1998). Epsin is an EH-domain-binding protein implicated in clathrin-mediated endocytosis. Nature 394, 793–797. 10.1038/29555. [PubMed: 9723620]
37. Rosendale M, Van TNN, Grillo-Bosch D, Sposini S, Claverie L, Gauthereau I, Claverol S, Choquet D, Sainlos M, and Perrais D (2019). Functional recruitment of dynamin requires multimeric interactions for efficient endocytosis. Nat. Commun. 10, 4462. 10.1038/s41467-019-12434-9. [PubMed: 31575863]
38. Daumke O, Roux A, and Haucke V (2014). BAR domain scaffolds in dynamin-mediated membrane fission. Cell 156, 882–892. 10.1016/j.cell.2014.02.017. [PubMed: 24581490]
39. Liu YW, Neumann S, Ramachandran R, Ferguson SM, Pucadyil TJ, and Schmid SL (2011). Differential curvature sensing and generating activities of dynamin isoforms provide opportunities for tissue-specific regulation. Proc. Natl. Acad. Sci. USA 108, E234–E242. 10.1073/pnas.1102710108. [PubMed: 21670293]
40. Bhave M, Mettlen M, Wang X, and Schmid SL (2020). Early and nonredundant functions of dynamin isoforms in clathrin-mediated endocytosis. Mol. Biol. Cell 31, 2035–2047. 10.1091/mbc.E20-06-0363. [PubMed: 32579424]
41. Taylor MJ, Lampe M, and Merrifield CJ (2012). A feedback loop between dynamin and actin recruitment during clathrin-mediated endocytosis. PLoS Biol. 10, e1001302. 10.1371/journal.pbio.1001302. [PubMed: 22505844]
42. Hussain NK, Jenna S, Glogauer M, Quinn CC, Wasiak S, Guipponi M, Antonarakis SE, Kay BK, Stossel TP, Lamarche-Vane N, and McPherson PS (2001). Endocytic protein intersectin-l regulates actin assembly via Cdc42 and N-WASP. Nat. Cell Biol. 3, 927–932. 10.1038/ncb1001-927. [PubMed: 11584276]
43. Pechstein A, Gerth F, Milosevic I, Jäpel M, Eichhorn-Grünig M, Vorontsova O, Bacetic J, Maritzen T, Shupliakov O, Freund C, and Haucke V (2015). Vesicle uncoating regulated by SH 3- SH 3 domain-mediated complex formation between endophilin and intersectin at synapses. EMBO Rep. 16, 232–239. 10.15252/embr.201439260. [PubMed: 25520322]
44. Keating DJ, Chen C, and Pritchard MA (2006). Alzheimer's disease and endocytic dysfunction: Clues from the Down syndrome-related proteins, DSCR1 and ITSN1. Ageing Res. Rev. 5, 388–401. 10.1016/j.arr.2005.11.001. [PubMed: 16442855]
45. Liaqat K, Treat K, Wilson TE, Conboy E, and Vetrini F (2024). Further evidence of involvement of ITSN1 in autosomal dominant neurodevelopmental disorder. Clin. Genet. 105, 455–456. 10.1111/cge.14497. [PubMed: 38346866]
46. Bruel AL, Vitobello A, Thiffault I, Manwaring L, Willing M, Agrawal PB, Bayat A, Kitzler TM, Brownstein CA, Genetti CA, et al. (2022). ITSN1: a novel candidate gene involved in autosomal dominant neurodevelopmental disorder spectrum. Eur. J. Hum. Genet. 30, 111–116. 10.1038/s41431-021-00985-9. [PubMed: 34707297]
47. Zhou X, Feliciano P, Shu C, Wang T, Astrovskaya I, Hall JB, Obiajulu JU, Wright JR, Murali SC, Xu SX, et al. (2022). Integrating de novo and inherited variants in 42,607 autism cases identifies mutations in new moderate-risk genes. Nat. Genet. 54, 1305–1319. 10.1038/s41588-022-01148-2. [PubMed: 35982159]
48. Groza T, Gomez FL, Mashhadi HH, Muñoz-Fuentes V, Gunes O, Wilson R, Cacheiro P, Frost A, Keskivali-Bond P, Vardal B, et al. (2023). The International Mouse Phenotyping Consortium: comprehensive knockout phenotyping underpinning the study of human disease. Nucleic Acids Res. 51, D1038–D1045. 10.1093/nar/gkac972. [PubMed: 36305825]

49. Gerth F, Jäpel M, Pechstein A, Kochlamazashvili G, Lehmann M, Puchkov D, Onofri F, Benfenati F, Nikonenko AG, Fredrich K, et al. (2017). Intersectin associates with synapsin and regulates its nanoscale localization and function. Proc. Natl. Acad. Sci. USA 114, 12057–12062. 10.1073/pnas.1715341114. [PubMed: 29078407]
50. Chan KMC, Arthur AL, Morstein J, Jin M, Bhat A, Schlesinger D, Son S, Stevens DA, Drubin DG, and Fletcher DA (2021). Evolutionarily related small viral fusogens hijack distinct but modular actin nucleation pathways to drive cell-cell fusion. Proc. Natl. Acad. Sci. USA 118, e2007526118. 10.1073/pnas.2007526118. [PubMed: 33443166]
51. Bryant DM, Datta A, Rodríguez-Fraticelli AE, Peränen J, Martín-Belmonte F, and Mostov KE (2010). A molecular network for de novo generation of the apical surface and lumen. Nat. Cell Biol. 12, 1035–1045. 10.1038/ncb2106. [PubMed: 20890297]
52. Schindelin J, Arganda-Carreras I, Frise E, Kaynig V, Longair M, Pietzsch T, Preibisch S, Rueden C, Saalfeld S, Schmid B, et al. (2012). Fiji: An open-source platform for biological-image analysis. Nat. Methods 9, 676–682. 10.1038/nmeth.2019. [PubMed: 22743772]
53. Grimm JB, Muthusamy AK, Liang Y, Brown TA, Lemon WC, Patel R, Lu R, Macklin JJ, Keller PJ, Ji N, and Lavis LD (2017). A general method to fine-tune fluorophores for live-cell and in vivo imaging. Nat. Methods 14, 987–994. 10.1038/nmeth.4403. [PubMed: 28869757]
54. Lemière J, Ren Y, and Berro J (2021). Rapid adaptation of endocytosis, exocytosis and eisosomes after an acute increase in membrane tension in yeast cells. Elife 10, 1–29. 10.1101/342030.
55. Berro J, and Pollard TD (2014). Local and global analysis of endocytic patch dynamics in fission yeast using a new “temporal superresolution” realignment method. Mol. Biol. Cell 25, 3501–3514. 10.1091/mbc.E13-01-0004. [PubMed: 25143395]

Highlights

- Intersectin1 (ITSN1) functions in CME site stabilization and growth rather than initiation
- ITSN1 is recruited to single CME sites at about half the level of dynamin2
- The EH and CC domains of ITSN1 are crucial for its recruitment to CME sites
- Through its SH3 domains, ITSN1 is essential for early- to mid-stage dynamin2 recruitment

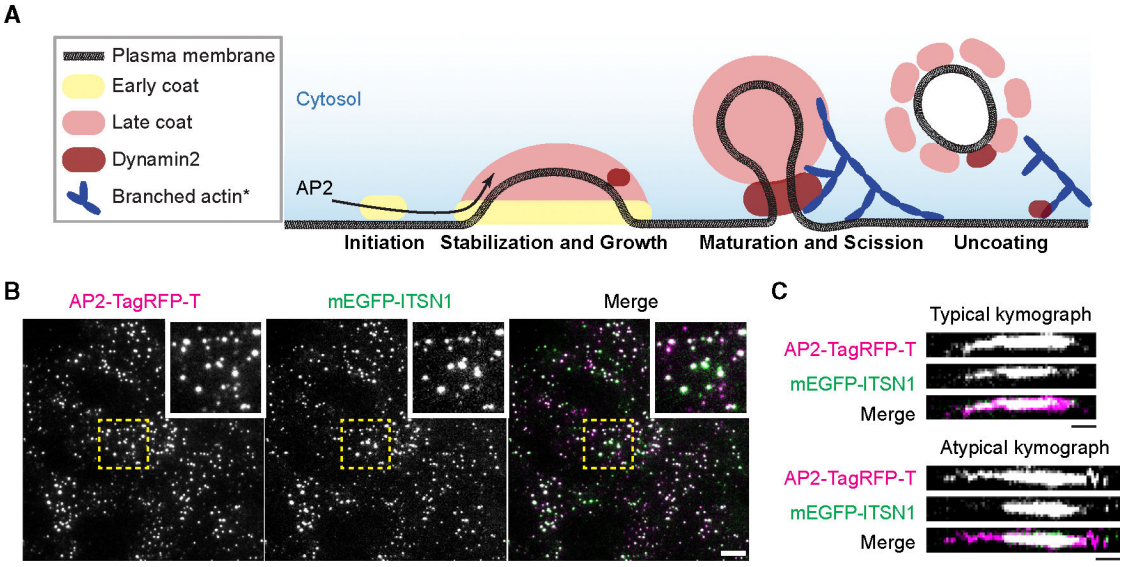

Figure 1. Endogenously labeled ITSN1 is recruited during the early to middle stage of CME

(A) Schematic model highlighting different stages of CME referred to in the text. *Branched actin filaments assemble at only some CME sites in hiPSCs.[15]

(B) A representative single-time-frame image from a TIRF video of AP2M1-tagRFP-T (magenta) and mEGFP-ITSN1 (green) genome-edited human iPSCs. The regions enlarged in the insets are boxed by the dashed lines. Scale bar: 5 μm.

(C) A typical and an atypical kymograph of CME sites in AP2M1-tagRFP-T (magenta) and mEGFP-ITSN1 (green) genome-edited human iPSCs. Scale bar: 10 s. See also Figure S1.

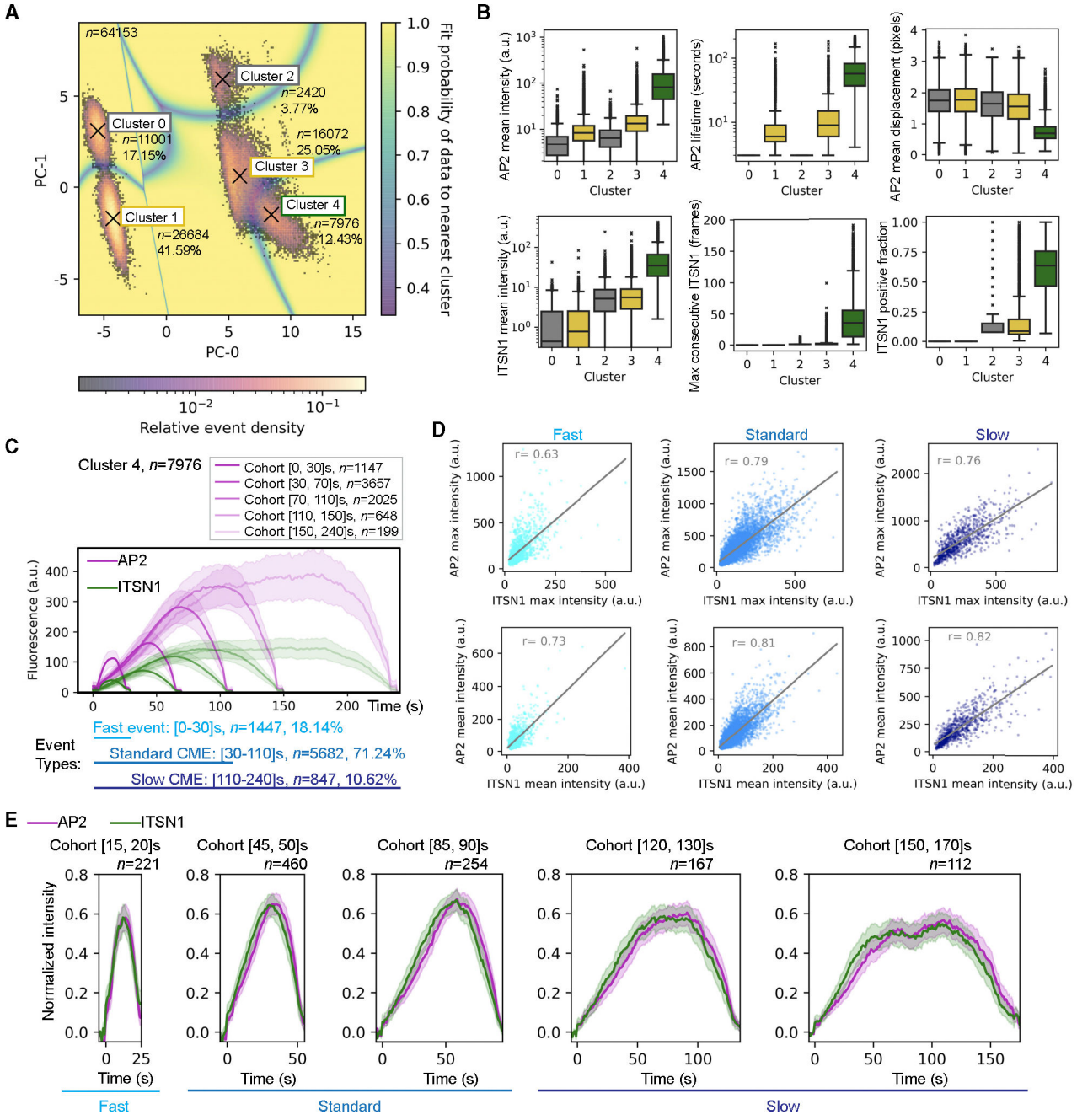

Figure 2. ITSN1 is recruited during the stabilization and growth stages of CME site assembly

(A) 2D histogram of the first two principal components (PCs) of AP2M1 and ITSN1 dynamic features. Valid tracks detected by cmeAnalysis[25] that appeared and disappeared during video acquisition and had lifetimes longer than 2 s were selected for the clustering. Relative event density shows the distribution of the valid tracks in the PC space, and the shaded underlay (fit probability of data to the nearest cluster) represents the probability of the simulated data points belonging to the nearest cluster. n = 64,153. The numbers and percentiles of the tracks in each individual cluster are shown.

(B) Quantification of ITSN1 and AP2 mean intensity, AP2 lifetime, mean displacement, maximum number of consecutive ITSN1 frame detections, and the fraction of the tracks with positive ITSN1 detection in valid tracks across different clusters. For boxplots, the box extends from the first quartile to the third quartile of the data, with a line at the median. Whiskers extend 1.5× the interquartile range (IQR) from the box. Outliers are shown as "x" marks. Cluster 0, n = 11,001; cluster 1, n = 26,684; cluster 2, n = 2,420; cluster 3, n = 16,072; cluster 4, n = 7,976.

(C) Averaged intensity vs. time plots for cohorts of cluster 4 tracks. Tracks are grouped into cohorts by AP2 lifetimes. Numbers of tracks in each cohort are shown in the figure. Data are represented as mean ± ¼ SD.

(D) Scatterplots of maximum (top) and average (bottom) intensities of ITSN1 and AP2 for different types of cluster 4 tracks. Each data point represents a track. The linear regression line is shown in gray. r, correlation coefficient. Fast events, n = 1,447; standard CME, n = 5,682; slow CME, n = 847.

(E) Averaged intensity vs. time plots for different lifetime cohorts of cluster 4 tracks. Tracks are grouped into cohorts based on AP2 lifetimes and aligned at the first detection of AP2 (time 0). Numbers of tracks in each cohort are shown in the figure. Data are represented as mean ± ¼ SD. The number of tracks in each cohort is shown in the plot.

See also Figure S2.

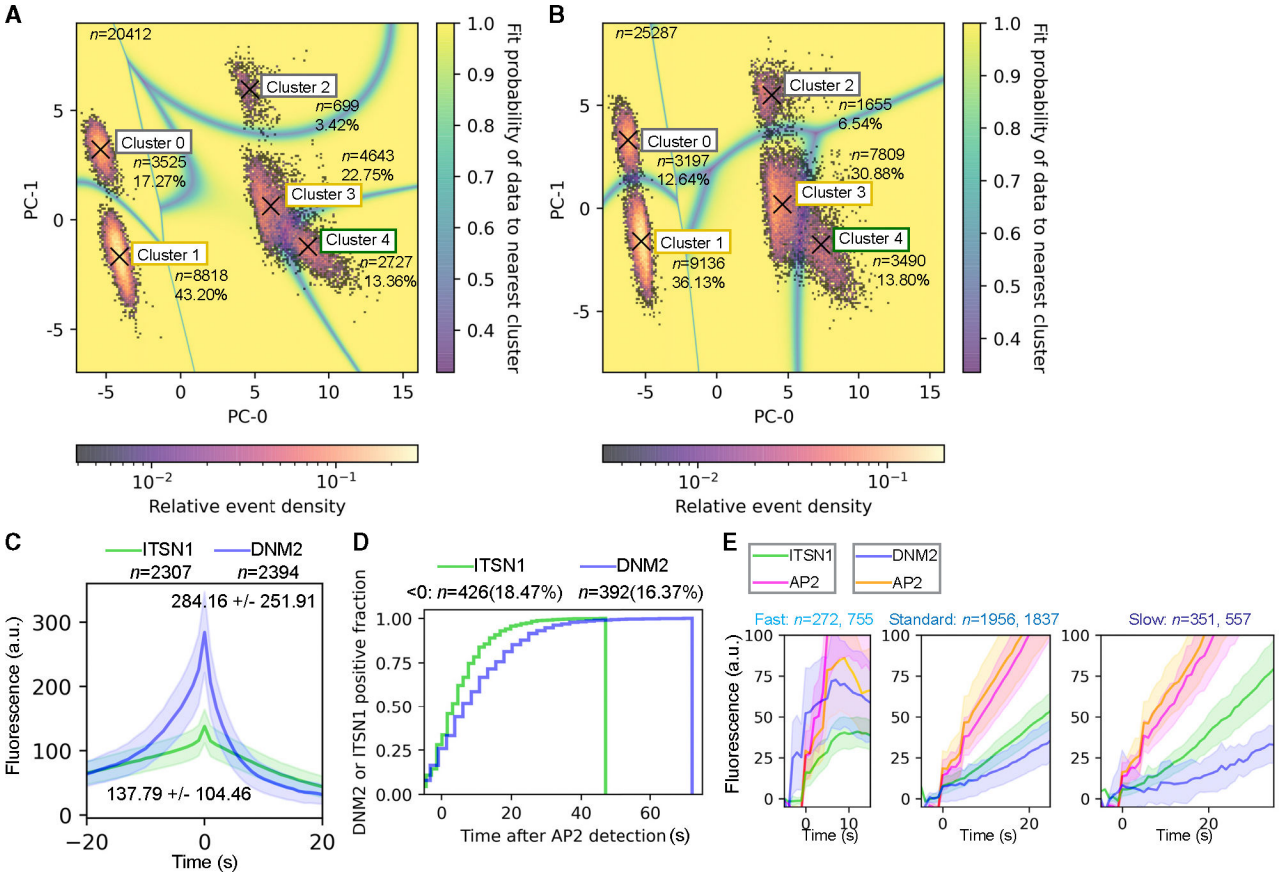

Figure 3. One to two dozen ITSN1 molecules are recruited to each CME site

(A and B) 2D histograms of the first two PCs forAP2 and ITSN1 (A) and AP2 and DNM2 (B). Shown are dynamic features extracted from live-cell imaging data collected on the same days using the same imaging parameters. Tracking and plotting methods are as described in Figure 2A. The figures show the numbers and percentiles of tracks in each individual cluster.

(C) Averaged intensity vs. time plots for ITSN1 and DNM2 in standard and slow CME events (cluster 4, lifetime ≥ 30 s with ≥ 5 consecutive frames of ITSN1 or DNM2 detections). Tracks are aligned at the ITSN1 or DNM2 peak (time 0). Note that AP2 intensities are not shown in the plot. Data are represented as mean ± ¼ SD. The number of tracks, along with the average and standard deviation of the maximum intensities of ITSN1 and DNM2, are displayed.

(D) Cumulative histogram of the fraction of ITSN1- or DNM2-positive standard and slow CME tracks (cluster 4, lifetime ≥ 30s with ≥ 5 consecutive frames of ITSN1 or DNM2 detections) at a given time after the AP2 signal is first detected (time 0). n = 2,307, 2,394.

(E) Averaged intensity vs. time plots for different event types of cluster 4 tracks. Tracks with equal to or more than 5 consecutive frames of ITSN1 or DNM2 detections are grouped based on AP2 lifetimes and aligned at the first detection of AP2 (time 0). Numbers of tracks in each type of events are shown. Data are represented as mean ± ¼ SD.

See also Figure S3.

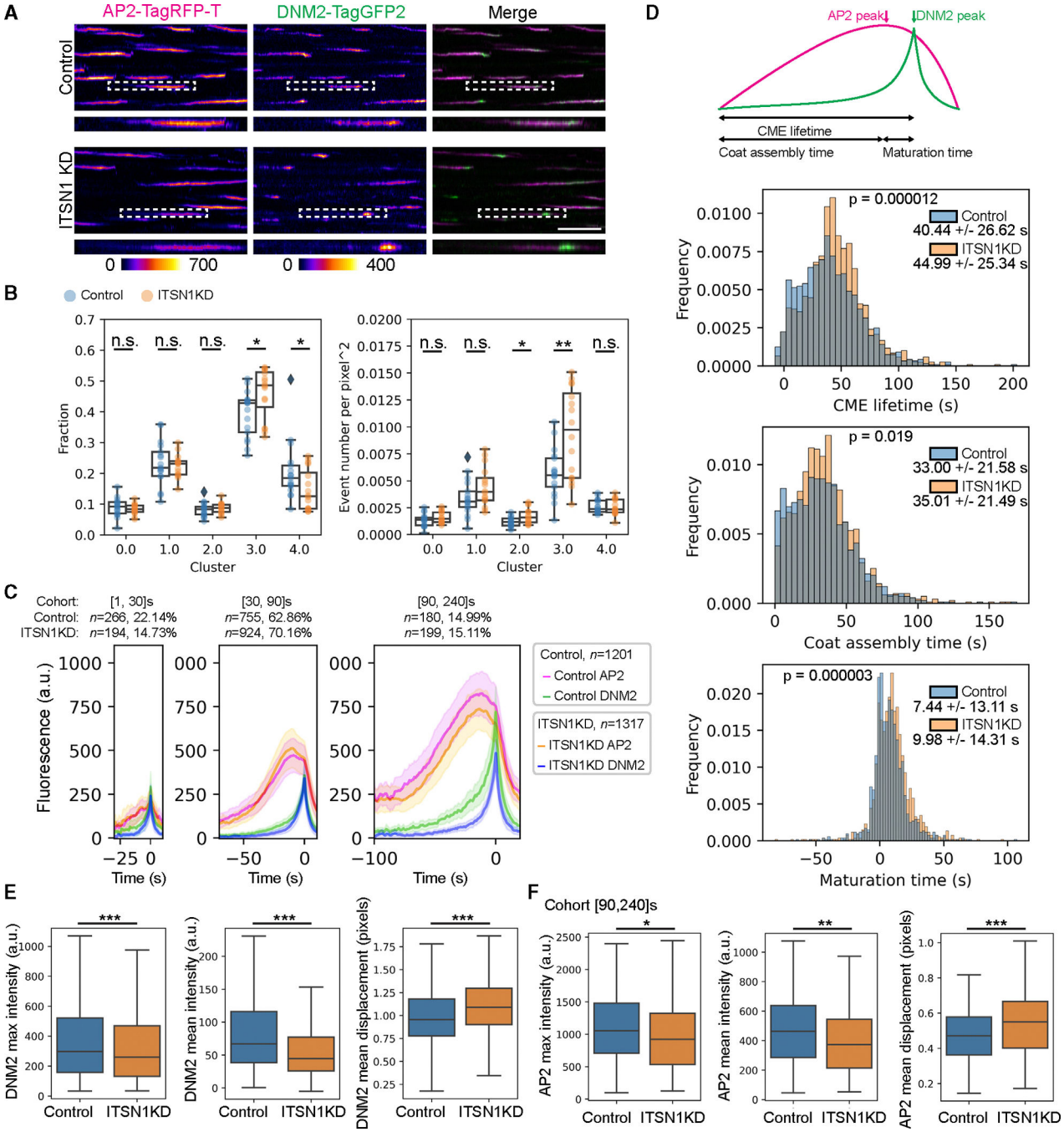

Figure 4. ITSN1 promotes CME site stabilization

(A) Representative kymographs of genome-edited AP2M1-tagRFP-T (magenta) and DNM-tagGFP2 (green) at CME sites in cells 2 days after transfection of plasmids expressing scramble (control) or ITSN1 shRNAs (ITSN1 KD). The highlighted kymograph is boxed by a dashed line. Scale bar: 60 s

(B) Quantification of fraction (left) and event density (right) of each cluster in the valid tracks detected in control and ITSN1 KD cells. Each data point represents a dataset collected from one cropped region of TIRF videos with shRNA transfection. For boxplots, the box

extends from the first quartile to the third quartile of the data, with a line at the median. Whiskers extend 1.5× the IQR from the box. Outliers are shown as diamond marks. Control, $n = 17$; ITSN1 KD, $n = 16$. Statistics: Welch's t test; n.s., not significant; $*p < 0.05$, $**p < 0.01$.

(C) Averaged intensity vs. time plots of cohorts of cluster 4 and DNM2-positive tracks of control and ITSN1 KD cells. Tracks are grouped into cohorts by the lifetimes of AP2. Tracks are aligned at the maximum intensity of DNM2 (time 0). The total number of tracks is shown to the right of the plots, and the number of tracks in each cohort is shown on the top of the plots. Data are represented as mean ± ¼ SD.

(D) Quantification of CME lifetime, coat assembly time, and maturation time of cluster 4 tracks in control and ITSN1 KD cells, presented as histograms. The diagram illustrates how the different time features were measured. Control, $n = 1{,}201$; ITSN1 KD, $n = 1{,}317$. Data are represented as mean ± SD. Statistics: Welch's t test.

(E) Quantification of DNM2 maximum intensity, mean intensity, and mean displacement of cluster 4 tracks in control and ITSN1 KD cells. For boxplots, the box extends from the first quartile to the third quartile of the data, with a line at the median. Whiskers extend 1.5× the IQR from the box. Note that outliers are not shown in the plots but are included in the statistical analysis. Control, $n = 1{,}201$; ITSN1 KD, $n = 1{,}317$. Statistics: Welch's t test, $***p < 0.005$.

(F) Quantification of AP2 maximum intensity, mean intensity, and mean displacement of cluster 4 tracks in the 90- to 240-s lifetime cohort in control and ITSN1 KD cells. The methods of plotting and statistics are the same as in (E). Control, $n = 180$; ITSN1 KD, $n = 199$. Statistics: Welch's t test, $*p < 0.05$, $**p < 0.01$, $***p < 0.005$.

See also Figure S4.

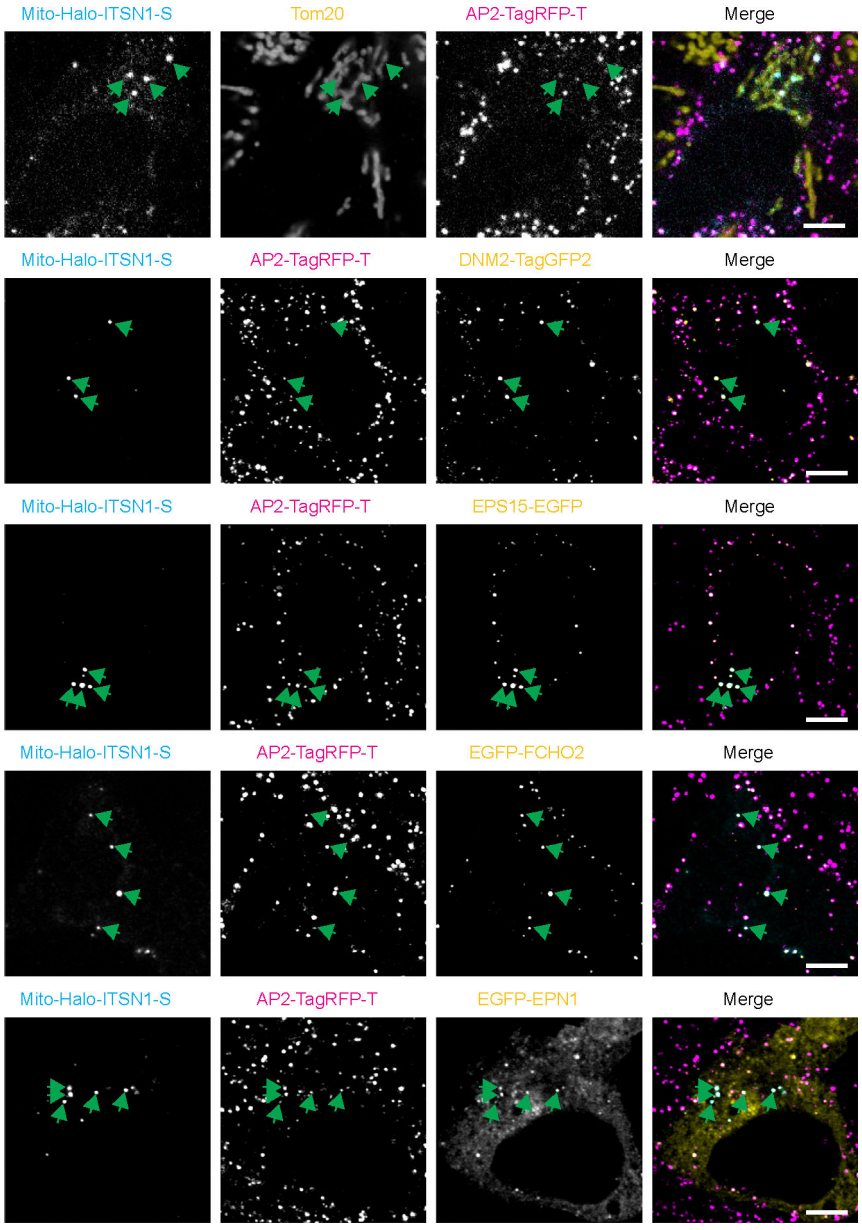

Figure 5. ITSN1 recruitment to mitochondria is sufficient to coalesce multiple endocytic proteins into mitochondrion-associated puncta

Representative cells fixed 2 days after ectopic mito-HaloTag-ITSN1-S transfection. Images are z stacks generated by maximum-intensity projection of 11 optical sections acquired using a Carl Zeiss Airyscan fluorescence microscope. AP2M1 and DNM2 were endogenously tagged with TagRFP-T and TagGFP2, respectively. Tom20 was labeled by immunofluorescence. Plasmids expressing fluorescent protein-conjugated EPS15, FCHO2, or EPN1 were co-transfected with the mito-HaloTag-ITSN1-S-expressing plasmid. Scale bar: 5 μm.

See also Figure S5.

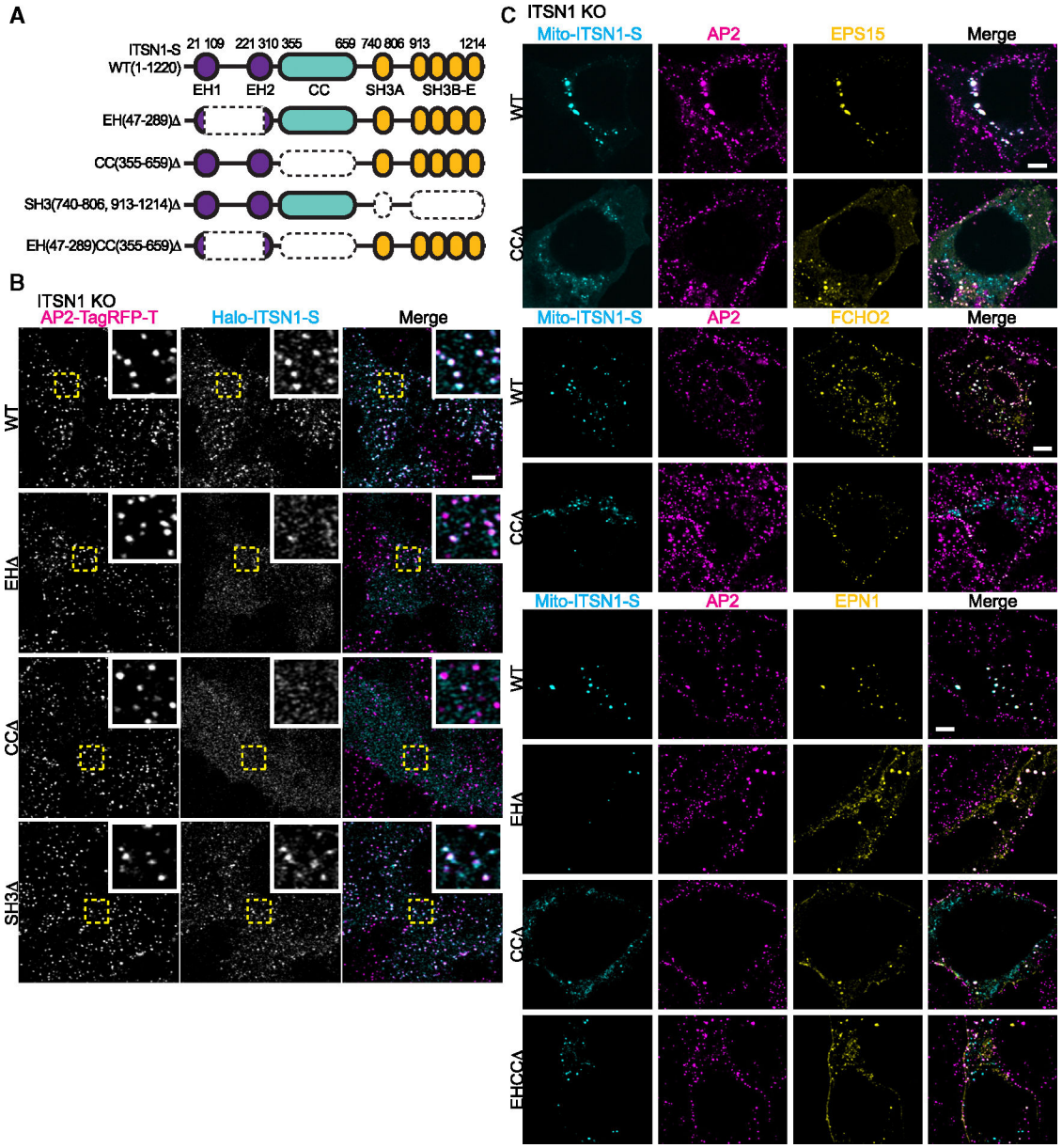

Figure 6. ITSN1's EH and CC domains play roles in ITNS1 recruitment to CME sites

(A) An illustration of domains of wild-type ITSN1-S and the truncation mutants investigated in this study.

(B) Representative cells fixed 2 days after transfection with plasmids expressing wild-type or a truncated form of mito-HaloTag-ITSN1-S. Images were acquired using a Carl Zeiss Airyscan fluorescence microscope. Single-stack images of the basal plasma membrane of cells, where CME sites are labeled by AP2M1-TagRFP-T, are shown. Scale bar: 5 μm.

(C) Representative images of puncta assembled by mitochondrial recruitment of wild-type or truncation forms of mito-HaloTag-ITSN1-S. Cells were fixed 2 days after plasmid transfection. AP2M1 was endogenously tagged with TagRFP-T. Plasmids expressing fluorescent protein-conjugated EPS15, FCHO2, or EPN1 were co-transfected with the mito-HaloTag-ITSN1-S-expressing plasmid. Images are z stacks generated by maximum-

intensity projection of 11 optical sections acquired using a Carl Zeiss Airyscan fluorescence microscope. Scale bar: 5 μm.
See also Figure S6.

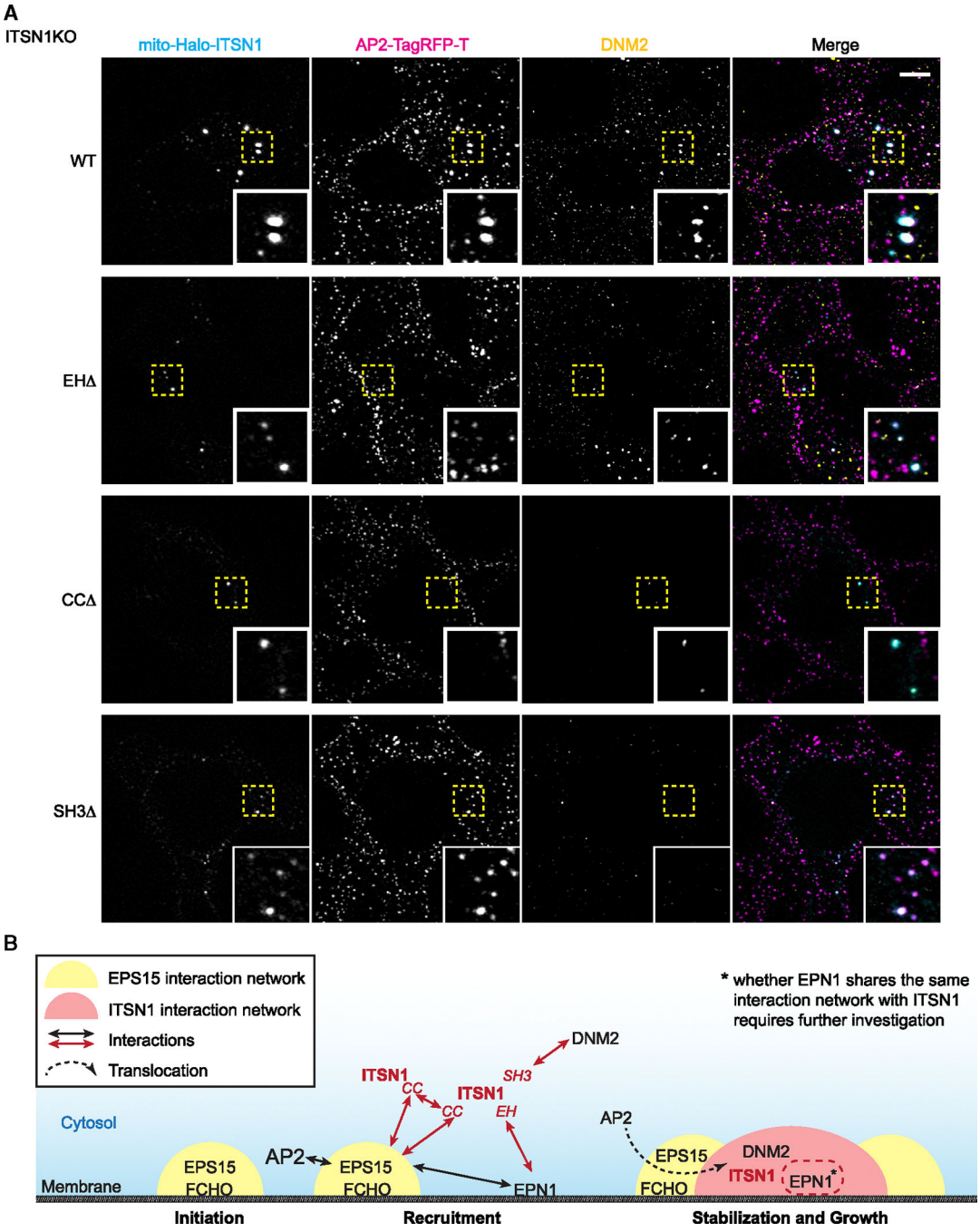

Figure 7. ITSN1's domains play distinctive roles in establishing its interaction network

(A) Representative puncta formed by wild-type and truncation forms of mito-HaloTag-ITSN1-S. AP2M1-TagRFP-T, ITSN1 KO genome-edited cells were fixed 2 days after plasmid transfection, and DNM2 was labeled by immunofluorescence. Cells were imaged using a Carl Zeiss Airyscan fluorescence microscope, and images were generated by maximum-intensity projection of 11 optical z sections. Scale bar: 5 μm.

(B) A schematic model for how ITSN1 is recruited to CME sites and how it stabilizes CME sites by forming an interaction network among endocytic proteins, including DNM2 and EPN1, which associates with the EPS15-FCHO-containing initiation condensate.
See also Figure S7.

KEY RESOURCES TABLE

REAGENT or RESOURCE	SOURCE	IDENTIFIER
Antibodies		
Anti-Tag(CGY)FP	Evrogen	Cat# AB121; RRID:AB_2716691
GAPDH antibody	Proteintech	Cat# 10494–1-AP; RRID:AB_2263076
TOM20 antibody	Proteintech	Cat# 11802–1-AP; RRID:AB_2207530
Dynamin2 antibody	Abcam	Cat# ab3457; RRID:AB_2093679
Goat anti-Rabbit IgG (H + L) Cross-Adsorbed Secondary Antibody, Alexa Fluor™ 488	Thermo Fisher Scientific	Cat# A11008; RRID:AB_143165
IRDye 800CW Goat anti-Rabbit IgG	LI-COR Biosciences	Cat# 926–32211; RRID:AB_621843
IRDye 800CW Goat anti-Mouse IgG	LI-COR Biosciences	Cat# 926–32210; RRID:AB_621842
Chemicals, peptides, and recombinant proteins		
PFA	Electron Microscopy Sciences	Cat# 15710
Y-27632	Chemdea	Cat# CD0141
Critical commercial assays		
Corning® Matrigel® hESC-Qualified Matrix	Sigma-Aldrich	Cat# CLS354277
StemFlex™ Medium	Thermo Fisher Scientific	Cat# A3349401
Gentle Cell Dissociation Reagent	StemCell Technologies	Cat# 100–0485
Lipofectamine™ Stem Transfection Reagent	Thermo Fisher Scientific	Cat# STEM00001
NEBuilder HiFi DNA Assembly Master Mix	New England Biolabs	Cat# E2621S
Human Stem Cell Nucleofector™ Kit 1	Lonza	Cat# VPH-5012
PhosSTOP	Roche	Cat# 4906845001
Protease inhibitor	Roche	Cat# 1183617001
PageRuler Plus Prestained Protein Ladder	Thermo Fisher Scientific	Cat# 26619
Deposited data		
Raw and analyzed data	This paper	Zenodo: http://doi.org/10.5281/zenodo.13737837
Experimental models: Cell lines		
Human: hiPSC line WTC	Laboratory of Bruce Conklin	Coriell Cat# GM25256; RRID:CVCL_Y803
Human: hiPSC line WTC AP2M1-tagRFP-t DNM2-tagGFP2	Jin et al.[15]	N/A
Human: hiPSC line WTC AP2M1-tagRFP-t mEGFP-ITSN1	Chan et al.[50]	N/A
Human: hiPSC pool WTC AP2M1-tagRFP-t ITSN1KO	This paper	N/A

REAGENT or RESOURCE	SOURCE	IDENTIFIER
Oligonucleotides		
sgRNA targeting sequence: ITSN1 N' knock in: AGGTGTTGGAAACTGAGCCA	This paper	N/A
sgRNA targeting sequence: EGFP-ITSN1 KO: GAAGTTCGAGGGCGACACCC	This paper	N/A
shRNA targeting sequence: ITSN1 KD-1: GATATCAGATGT CGATTGA	This paper	N/A
shRNA targeting sequence: ITSN1 KD-2: GGACATAGTTGTACTGAAA	This paper	N/A
Non-targeting shRNA sequence: scramble: CCTAAGGTTAAGTCGCCCTCG	Bryant et al.[51]	N/A
Recombinant DNA		
Plasmid: HaloTag-ITSN1-S	This paper	N/A
Plasmid: mito-HaloTag-ITSN1-S	This paper	N/A
Plasmid: mito-HaloTag-EPS15	This paper	N/A
Plasmid: mito-EGFP-ITSN1-S	This paper	N/A
Plasmid: HaloTag-ITSN1-EHΔ	This paper	N/A
Plasmid: HaloTag-ITSN1-CCΔ	This paper	N/A
Plasmid: HaloTag-ITSN1-SH3Δ	This paper	N/A
Plasmid: mito-HaloTag-ITSN1-EHΔ	This paper	N/A
Plasmid: mito-HaloTag-ITSN1-CCΔ	This paper	N/A
Plasmid: mito-HaloTag-ITSN1-EHCCΔ	This paper	N/A
Plasmid: mito-HaloTag-ITSN1-SH3Δ	This paper	N/A
Plasmid: EPS15-EGFP (human)	Sochacki et al.[12]	N/A
Plasmid: EGFP-FCHO2 (mouse)	Henne et al.[6]	N/A
Plasmid: EGFP-EPN1 (rat)	Chen et al.[36]	RRID:Addgene_22228
Plasmid: pSuper-scramble shRNA-2A-tagBFP	This paper	N/A
Plasmid: pSuper-ITSN1 shRNA1–2A-tagBFP	This paper	N/A
Plasmid: pSuper-ITSN1 shRNA2–2A-tagBFP	This paper	N/A
Software and algorithms		
Fiji	Schindelin et al.[52]	RRID:SCR_002285
MATLAB	N/A	RRID:SCR_001622
Python	N/A	RRID:SCR_008394
CmeAnalysis	Aguet et al.[25]	GitHub: https://github.com/DanuserLab/cmeAnalysis
FRAP analysis code	This paper	Zenodo: http://doi.org/10.5281/zenodo.13737779
TIRF image analysis code	This paper	Zenodo: http://doi.org/10.5281/zenodo.13737779